Morphological Classification of Luminous Infrared Galaxies in GOALS

William Meynardie

Instructor: Dr. Aaron Evans,
with help from Dr. Sean Linden

Department of Astronomy
University of Virginia

This thesis is submitted in partial completion of the requirements of the BS Astronomy-Physics major.

May 13, 2022

Abstract

Luminous Infrared Galaxies (LIRGs) are massive starbursts, typically composed of two or more galaxies at some stage of a galaxy merger. LIRGs dominate the infrared luminosity density at high redshift, so studying nearby LIRGs can give us insight into galaxies at high redshift. We analyze HST ACS/WFC images of a sample of 56 LIRGs by computing their Gini coefficient and M_{20} value at F435W (B-band) and F814W (I-band), and we use these results to classify the galaxies as mergers or non-mergers. We present the results of this analysis, and then sort the galaxies by a variety of parameters to identify trends in the data. Additionally, we analyzed the individual components of widely separated galaxies, expanding our sample to 85 individual components, and we note differences in trends compared to widely separated systems that were analyzed using images that contained both components. We find that the I-band is a better metric for classifying LIRGs as mergers via Gini-M_{20} analysis, and that very early and very late stage mergers are often classified as non-mergers. Based on our analysis, Gini-M_{20} merger classifications of high-redshift galaxies may be challenging for widely separated pairs and will be less accurate for rest-frame 0.4 μm images.

1 Background

Luminous Infrared Galaxies (LIRGs), defined as objects with $L_{\rm IR}$(8-1000 μm) $\geq 10^{11} L_{\odot}$, are massive starbursts which are bright at infrared wavelengths, often as a result of a galaxy merger (Sanders & Mirabel 1996).

LIRGs dominate the infrared luminosity density at high redshift (Murphy et al. 2011). One of the challenges with the interpretation of galaxies in the distant universe is classifying their morphologies to determine at what stage of interaction the galaxies are in the merger, or to determine if there is any interaction taking place at all. One method that has been adopted to solve this problem, developed by Lotz et al. (2008), relies on two parameters which characterize the light distribution – the Gini coefficient and the M_{20} value. The Gini coefficient is a measure of the inequality of the light distribution in a galaxy, while the M_{20} value measures the spatial distribution of the light. The advantage to this analysis is that it is purely quantitative, meaning that it is not subject to human biases and can be applied to any image of a galaxy where the individual components can be resolved.

A Gini-M_{20} analysis on a sample of nearby LIRGs was done by Petty et al. (2014) to further test the robustness of the technique on high-resolution HST data from the Great Observatories All-sky LIRG Survey (GOALS) sample (Armus et al. 2009). Petty et al. (2014) found that Gini-M_{20} was effective at classifying merging LIRGs as mergers, but their multiwavelength analysis was limited by the small field of view of the ACS/SBC far-UV observations. Here we focus only on the wide-field HST ACS/WFC F435W (B-band) and F814W (I-band) to capture the full extent of the mergers. Doing so allows us to expand the sample from 20 systems to 56 systems.

1.1 Gini Coefficient

The Gini coefficient is a metric invented by economists to measure inequality in a nation's wealth distribution (Gini 1912). A nation with perfect wealth equality has a Gini coefficient of 0, while a nation in which all of the wealth is owned by a single individual has a Gini coefficient approaching 1.

Analogously, the Gini coefficient has been used in astronomy to measure inequality in a galaxy's light distribution. An image with light distributed equally to each pixel has a Gini coefficient of 0, whereas an image in which all of the light is concentrated in a single pixel has a Gini coefficient approaching 1.

Quantitatively, the Gini coefficient is given by Equation 1 below, where f_i is the flux in pixel i from n total pixels, and $\bar{f}$ is the average flux (e.g. Petty et al. 2014). The pixels are sorted in order of increasing flux, so that $f_{i+1} \geq f_i$ for all i.

$$G = \frac{1}{|\bar{f}|n(n-1)} \sum_{i=1}^{n} (2i - n - 1)|f_i| \qquad (1)$$

1.2 M_{20} Value

The M_{20} value is defined as the logarithmic ratio giving the normalized second-order moment of the brightest pixels whose flux adds to 20% of the galaxy's total flux. It is given by Equation 2 below (Lotz et al. 2004).

$$M_{20} = \log_{10}\left(\frac{\sum_i M_i}{M_{tot}}\right) \qquad (2)$$

$\sum_i M_i$ is the sum of the M_i values for the brightest pixels which add to 20% of the total flux, where each M_i is given by Equation 3 below.

$$M_i = f_i\left[(x_i - x_c)^2 + (y_i - y_c)^2\right] \qquad (3)$$

The x and y coordinates of pixel i are given by x_i and y_i, and the x and y coordinates of the center of the galaxy are given by x_c and y_c. It is important to note that, while the Gini coefficient has no position dependence, the M_{20} value is dependent on where we define the center of the galaxy to be. Thus, the way we define the center of each system will be very important to our results.

2 Sample Selection

Our initial sample was composed of 88 LIRGs from the GOALS sample. GOALS is a complete sample of galaxies from the IRAS Revised Bright Galaxy Sample with 60 μm flux densities greater than 5.24 Jy (Sanders et al. 2003). The 88 galaxies in our sample are the LIRGs in GOALS with $L_{\mathrm{IR}} > 10^{11.4}\ L_{\odot}$ (Kim et al. 2013). We analyzed the HST ACS/WFC F435W (B-band) and F814W (I-band) images of each galaxy. Systems of three or more galaxies were omitted, as were systems which were highly contaminated by background stars. Four systems were omitted because they contained more than two galaxies, and 28 systems were omitted due to background contamination. In total, our sample consisted of 56 galaxies.

3 Data Analysis

As we highlighted in the first section, the first task for each system was to define the center. To do this, we placed an aperture between 0.2-0.9″ around the brightest central region of the galaxy's I-band image and picked out the brightest pixel in the aperture. We defined this pixel to be the center pixel.

In systems composed of two clearly separated galaxies, we defined the center to be the geometric midpoint of the centers of the two separated galaxies.

Finally, we trimmed the images to eliminate the effect of background sky as much as possible. For each system, we defined a cutoff value which was the median of the background sky plus 2.5 standard deviations of the sky pixels, and we set any value below this cutoff value to zero. This technique removed nearly all of the background sky pixels, while retaining nearly of the pixels in the source. We then cut each image in a square which was centered on the center of the galaxy and which contained the full extent of the galaxy. With the centers selected and the images trimmed, we calculated the Gini and M_{20} values of each of the systems.

3.1 Uncertainties

There are a few clear sources of error in these measurements. The first is the presence of background stars, as mentioned in Section 2. Background stars can appear very bright in the images, and when they show up on the edges of the image, they can drive the M_{20} value closer to 0. To address this, we removed systems which appeared to be highly contaminated by background stars from the sample. We made this judgement based on the number of stars, the brightness of the stars, and the brightness of the stars relative to the source. A few examples of systems that were removed from the sample are shown in Figures 1-3 below.

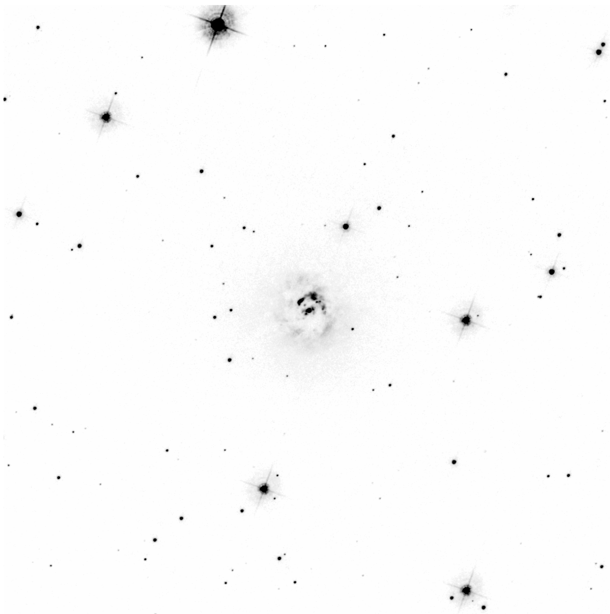

Figure 1: B-band image of IRAS 12116-5615. The image is highly contaminated by background stars.

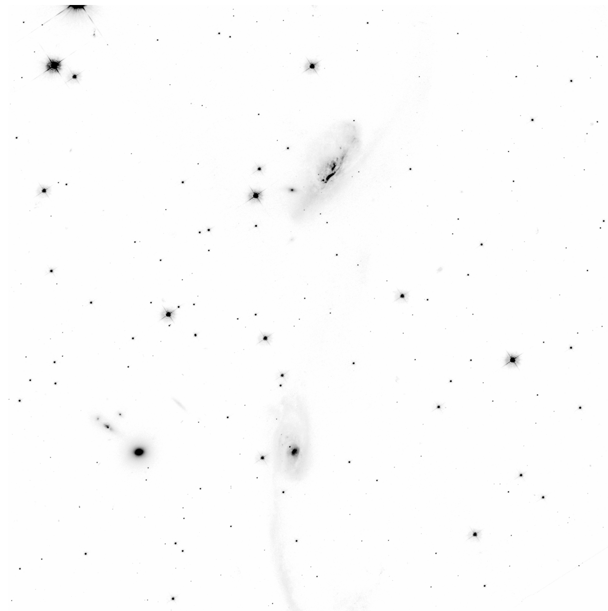

Figure 3: B-band image of ESO 069-IG 006. The image is highly contaminated by background stars.

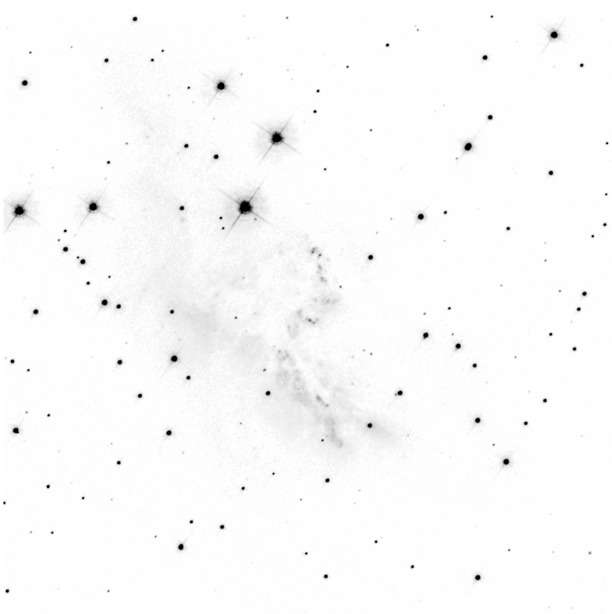

Figure 2: B-band image of ESO 099-G 004. The image is highly contaminated by background stars.

The main source of uncertainty for the M_{20} value lies in determining the position of the center pixel. To measure this uncertainty, we shifted the center pixel by 5% of the image size in eight directions to measure how the M_{20} value changes. We used the extrema of these tests as the upper and lower uncertainties.

We determined that the standard error in the Gini coefficient was negligible because each image had an average of about one million pixels. This large sample size drives the error in the Gini coefficient very close to zero. However, there is some intrinsic error due to the binning and image size. According to Petty et al. (2014), this error is ± 0.045.

Petty et al. (2014) also determined that the binning and image size causes an error of ± 0.1 for the M_{20} value, and this error is added in quadrature to the error determined from shifting the center pixel.

4 Results and Discussion

A plot of the positions of each image in Gini-M_{20} space is given in Figure 4 below. In the Figure, the blue data points represent the B-band images and the red data points represent the I-band images. The lines dividing the three classification regions are given by the blue and orange diagonal lines.

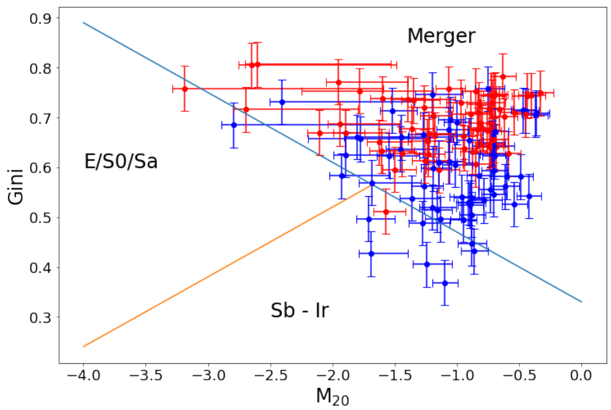

Figure 4: B-band (blue) and I-band (red) images of the galaxy sample in Gini-M_{20} space.

We find that the data points very clearly clump in the merger region of Gini-M_{20} space, consistent with the results from Lotz et al. (2008) and Petty et al. (2014). Given the merger nature of LIRGs, this is a confirmation of the accuracy of this technique.

4.1 Examples

Most of the data points fall in the merger region of Gini-M_{20} space. The galaxies classified as mergers broadly contain three types of galaxies: systems with a single component, galaxies with highly disturbed morphologies, and systems with multiple widely separated components. In this subsection, we will analyze a few of these galaxies that are representative of the larger sample.

First, we examine MCG-03-04-014. Its B-band image is shown in Figure 5 below, along with its position in Gini-M_{20} space.

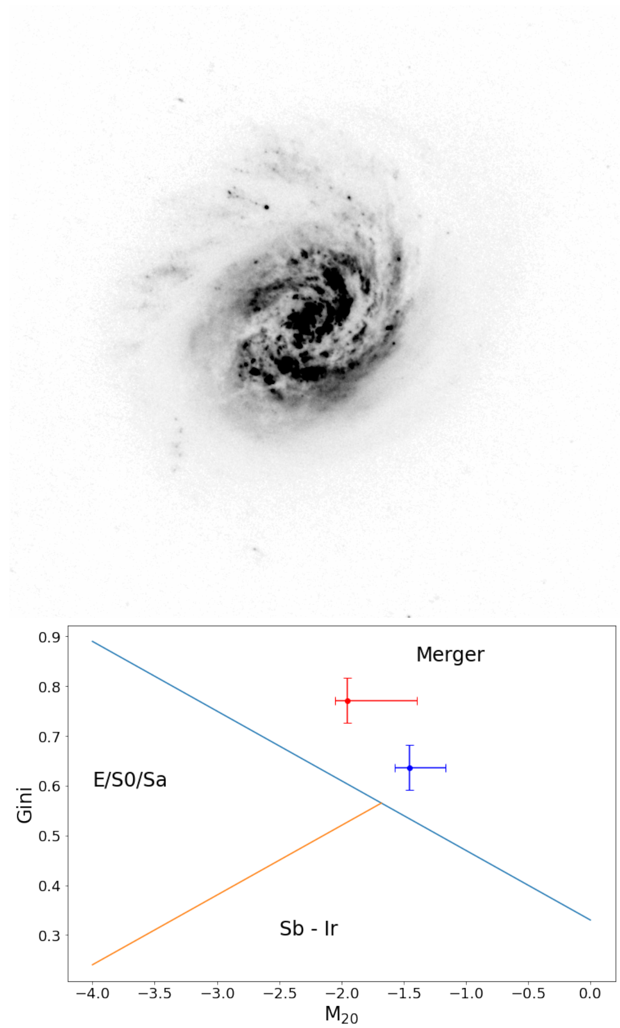

Figure 5: B-band image of MCG-03-04-014 (top), along with its B-band (blue) and I-band (red) position in Gini-M_{20} space (bottom).

About 43% of the galaxies in the sample, including MCG-03-04-014, appear as a single system; however, they often have pockets of increased emission far outside the nucleus, indicating increased star formation activity, likely due to a merger. These pockets of emission drive the M_{20} value closer to zero, and the high surface brightness increases the Gini coefficient, which causes these galaxies to fall neatly in the merger region.

Another galaxy representative of a larger group is NGC 3690. Its B-band image is shown in Figure 6 below, along with its position in Gini-M_{20} space.

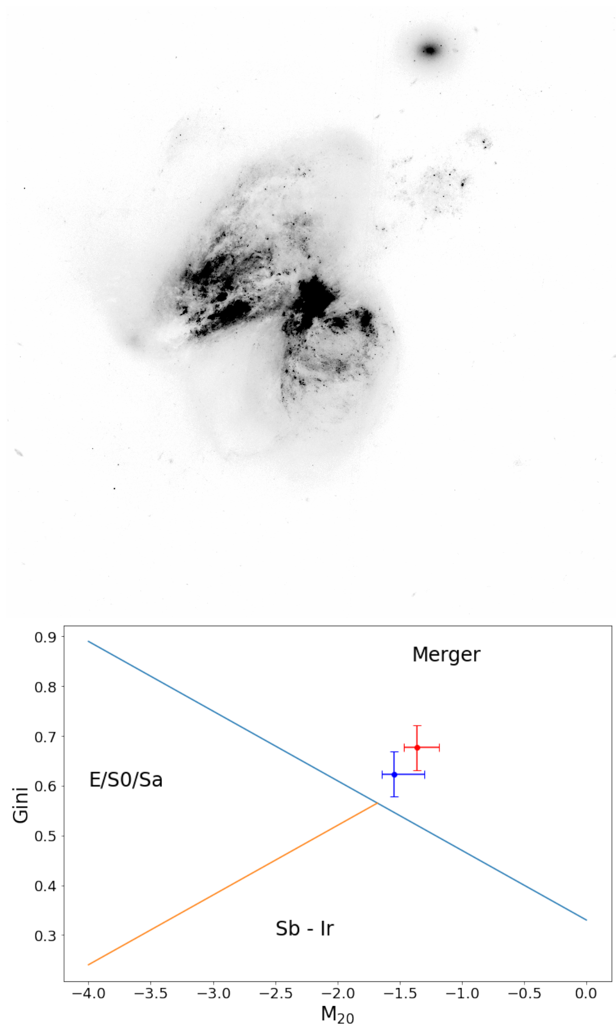

Figure 6: B-band image of NGC 3690 (top), along with its B-band (blue) and I-band (red) position in Gini-M_{20} space (bottom).

About 36% of the sample has a highly irregular shape, like NGC 3690. Like the previous example, the increased emission outside the nucleus and high surface brightness cause this galaxy to be classified as a merger.

Lastly, many of the galaxies in the sample resemble Arp 240. Its B-band image is shown in Figure 7 below, along with its position in Gini-M_{20} space.

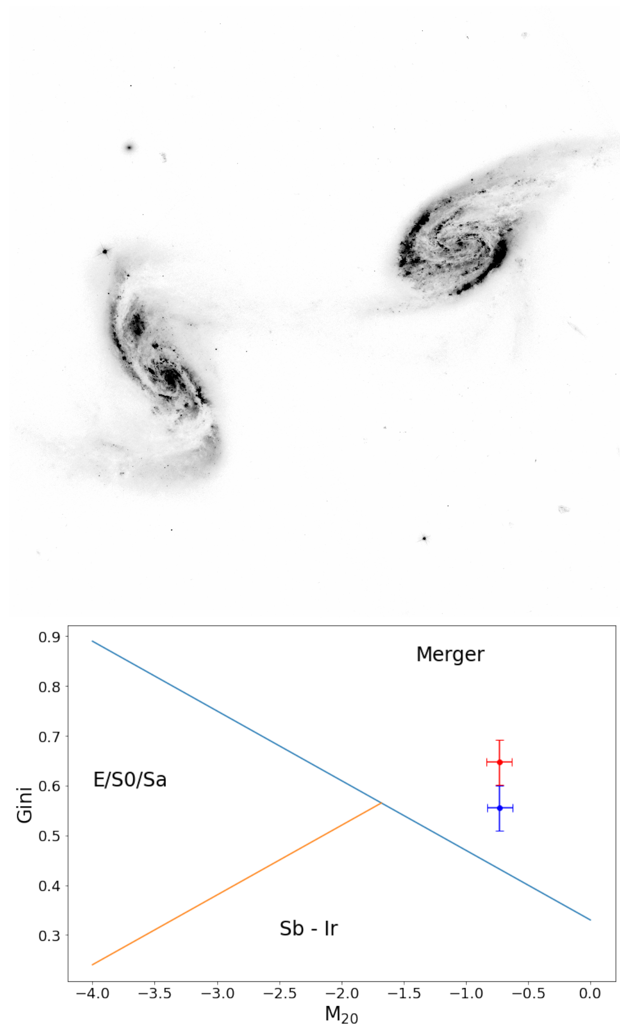

Figure 7: B-band image of Arp 240 (top), along with its B-band (blue) and I-band (red) position in Gini-M_{20} space (bottom).

The remaining 21% of galaxies in the sample, like Arp 240, are very clearly two separated systems, and so the bulk of the emission is coming from far outside the center of the image. This pushes the M_{20} value very close to zero, and these galaxies are easily classified as mergers.

4.2 Outliers

Although most of the data points fall in the merger region, there are a few data points which fall outside, and it is useful to analyze each of these individually.

The first of these is IRAS F05189-2524, which falls in the E/S0/Sa region in both the B-band and the I-band. These images are shown in Figure 8 below, along with their positions in Gini-M_{20} space.

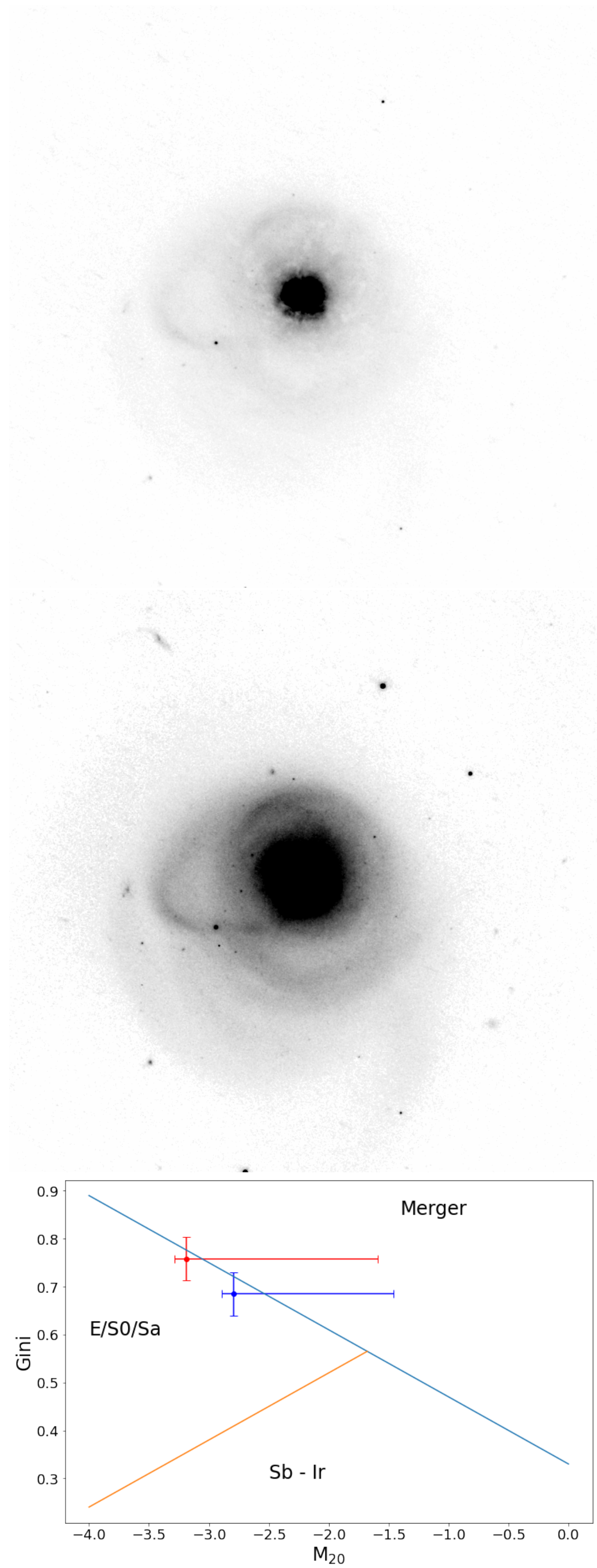

Figure 8: B-band image (top) and I-band image (middle) of IRAS F05189-2524, along with its B-band (blue) and I-band (red) position in Gini-M_{20} space (bottom).

This galaxy appears to be a late-stage merger. These images have the lowest M_{20} values of the entire sample, indicating that the brightest flux is mostly concentrated in the center. It is mostly spherical, with a few tidal features that indicate it has not fully merged. The large error bars indicate that its M_{20} value is highly sensitive to the position of the center pixel. This is because of how highly concentrated the flux is in the center.

The next outlier is IRAS F14378-3651, which falls in the Sb - Ir region in the B-band. This image is shown in Figure 9 below, along with its position in Gini-M_{20} space.

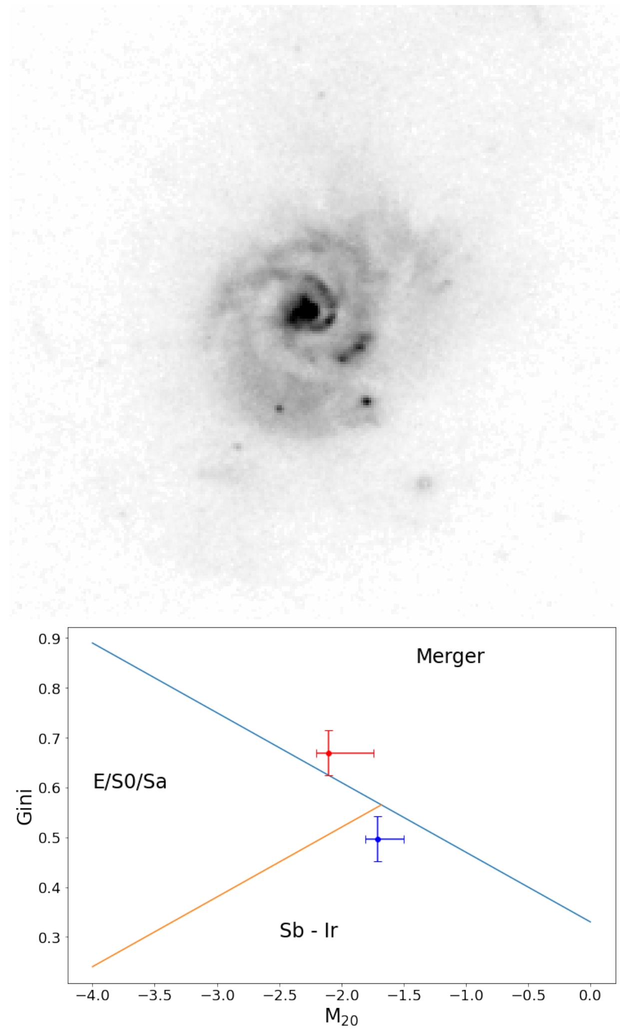

Figure 9: B-band image of IRAS F14378-3651 (top), along with its B-band (blue) and I-band (red) position in Gini-M_{20} space (bottom).

This galaxy appears to be mostly spiral in structure, so it is unsurprising that it falls in the Sb - Ir region. There appears to be some amount of low-level emission that survives the cutoff, and this may be driving the Gini coefficient downward. Additionally, there are a few pockets of emission outside the nucleus, and this is likely what drives the M_{20} value closer to zero.

The next galaxy is VV 705, which falls in the E/S0/Sa region in the B-band. This image is shown in Figure 10 below.

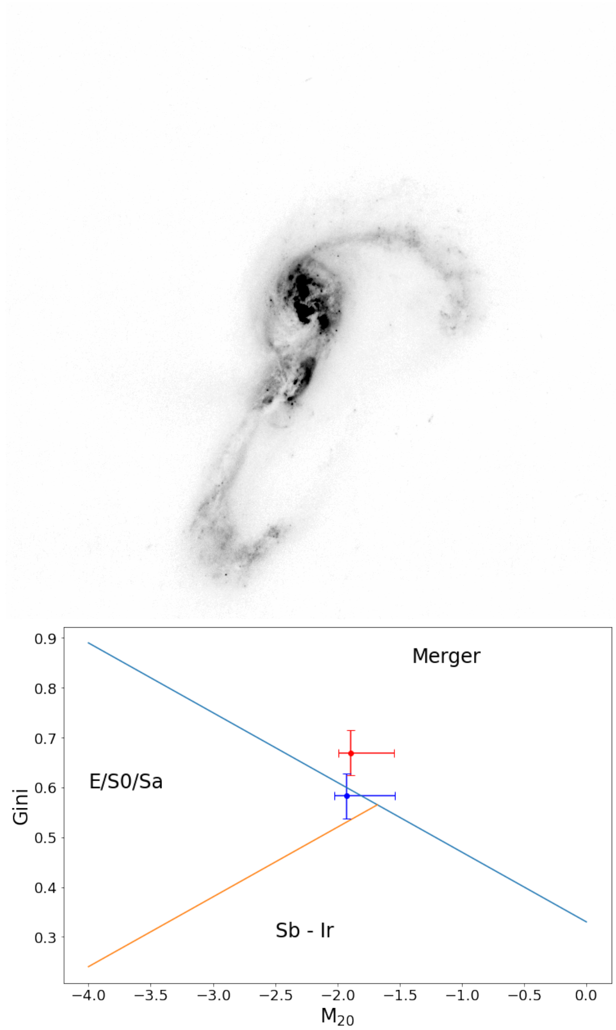

Figure 10: B-band image of VV 705 (top), along with its B-band (blue) and I-band (red) position in Gini-M_{20} space (bottom).

This galaxy is clearly a merger, with very prominent tidal features. The low surface brightness of the tidal tails is likely what drives the Gini coefficient downward. This data point is very close to the cutoff for mergers, but it is still surprising that this galaxy is not classified as a merger in the B-band.

The final set of outliers is IRAS F08572+3915, CGCG 043-099, ESO 057-G 070, UGC 09913, IRAS F16164-0746, and IRAS F16399-0937, for which the B-band images fall in the Sb - Ir region. These images, along with each galaxy's position in Gini-M_{20} space, are shown in Figure 11 below.

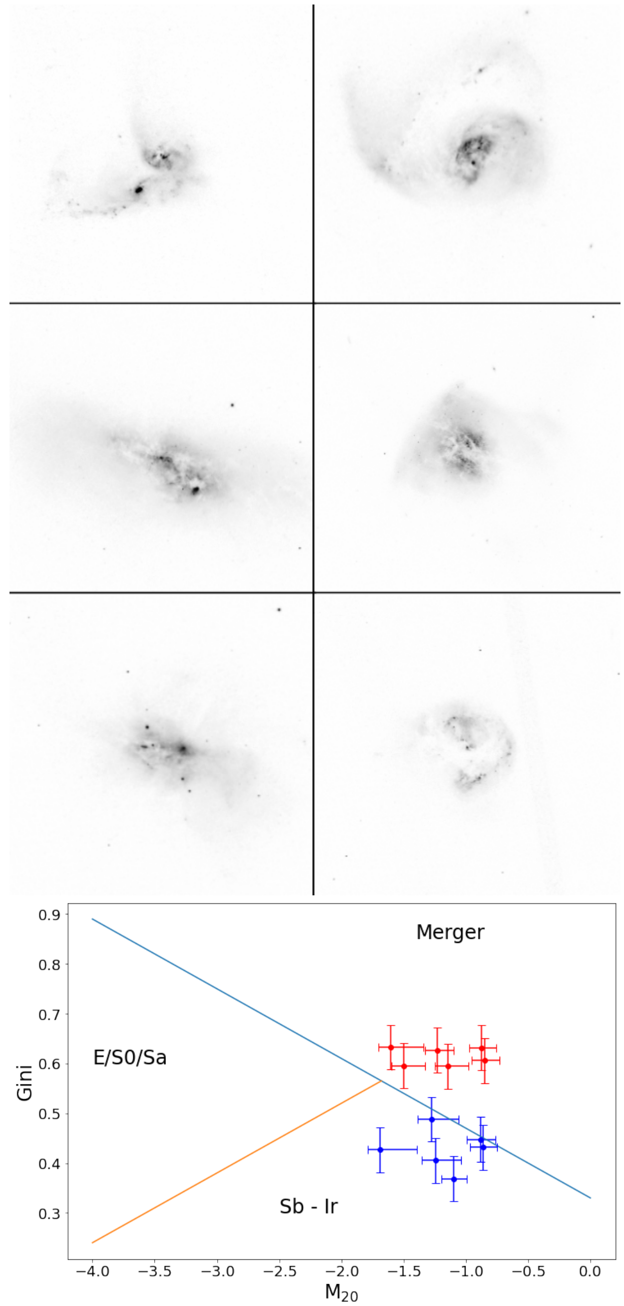

Figure 11: B-band images of IRAS F08572+3915 (top-left), CGCG 043-099 (top-right), ESO 057-G 070 (middle-left), UGC 09913 (middle-right), IRAS F16164-0746 (bottom-left), IRAS F16399-0937 (bottom-right) along with each of their B-band (blue) and I-band (red) positions in Gini-M_{20} space (bottom).

These galaxies are grouped together because each of them has significantly low surface brightness emission, which drives the Gini coefficient downward. Some of these, like IRAS F08572+3915, show clear distortion features, but these aren't enough to overcome the low Gini coefficient. IRAS F08572+3915, UGC 09913, and IRAS F16164-0746 are all very close to the merger region, but fall in the Sb - Ir region because of their low surface brightness. Despite the low surface brightness, each of these galaxies is classified as a merger in the I-band, and there is very little spread in their positions in Gini-M_{20} space.

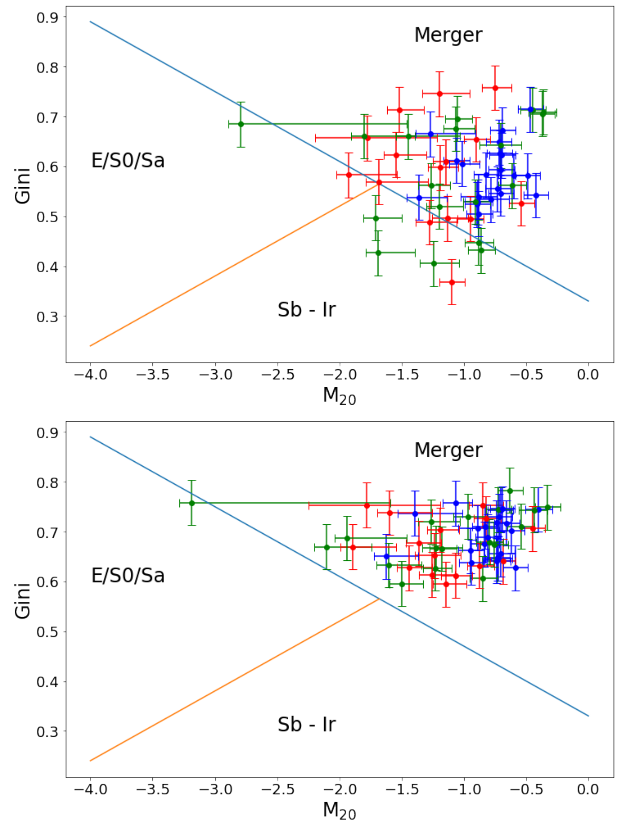

Figure 12: B-band plot (top) and I-band plot (bottom) of the sample, sorted by merger stage. Stage 1-2 is colored blue, stage 3-4 is colored red, and stage 5-6 is colored green.

4.3 Merger Stage

We sorted the data by a variety of different parameters to identify larger trends in the data. The first of the parameters we sorted by is the system's merger stage, given in Haan et al. (2011). Merger stage ranges from 0 to 6. Lower numbers indicate early stages of a merger, while higher numbers indicate later stages. Our plots of the sample sorted by merger stage are given in Figure 12 below.

The clearest trend we see is that early stage mergers clump towards M_{20} values close to zero. This is because of the wide separation between galaxies in these images. As the galaxies move to later stages in the merger, we find more scatter in the M_{20} value.

4.4 Molecular Gas Fraction

Next, we sorted the galaxies by molecular gas fraction (MGF), derived by Larson et al. (2016) for 25 of the galaxies in the sample. These plots are given in Figure 13 below.

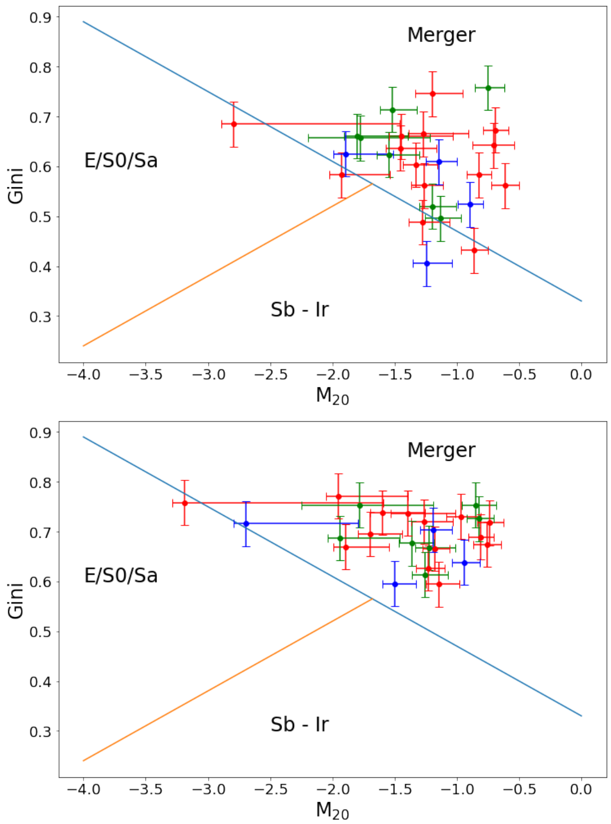

Figure 13: B-band plot (top) and I-band plot (bottom) of the sample, sorted by molecular gas fraction. 0-15% is colored blue, 15-30% is colored red, and over 30% is colored green. This sample contained 25 systems.

We examined this parameter because higher MGF tends to correlate with a higher degree of clumps in a galaxy's disk at high-redshift (Livermore et al. 2015). Despite this, we determined no significant trend in this data.

4.5 Separated Galaxies

Next, we separated early stage mergers into their individual components. We plotted each component from the sample individually, and only included multiple components in the same image if they were impossible to separate. The systems with more than two components have been added back into the sample for these plots, as well as components of widely separated systems for which only one of the components was contaminated by background stars. Our new sample contained 85 components. These plots are given in Figure 14 below.

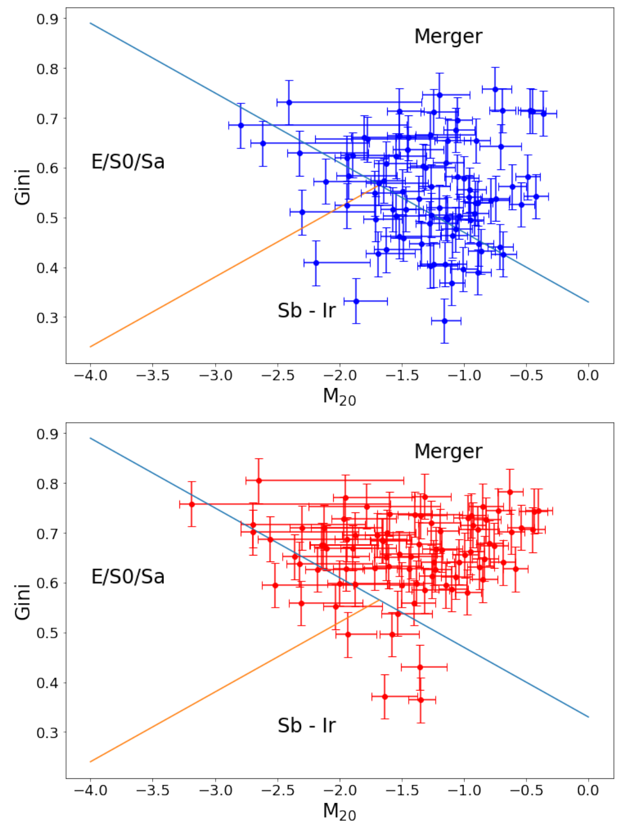

Figure 14: B-band plot (top) and I-band plot (bottom) of the sample, with individual components separated.

We find that many of these components fall far outside the merger region, especially in the B-band. Most of the components in the systems with more than two components are outliers. We can conclude that in these systems, if we did not see the components interacting, this technique would not be able to tell us that these components are part of a merger. This effect may impact analysis of galaxies at high redshift, because the physical resolution for high-redshift galaxies is inherently low.

4.6 Physical Separation

We next sorted the components by the physical separation between the two nuclei. In cases with three or more components, a component's physical separation to the other components was defined as the average of the distances to each of the other components. We calculated physical separation by measuring angular separation and deriving an angular scale based on the redshift given in the NED database.

Our plots of the components sorted by physical separation are given in Figure 15 below.

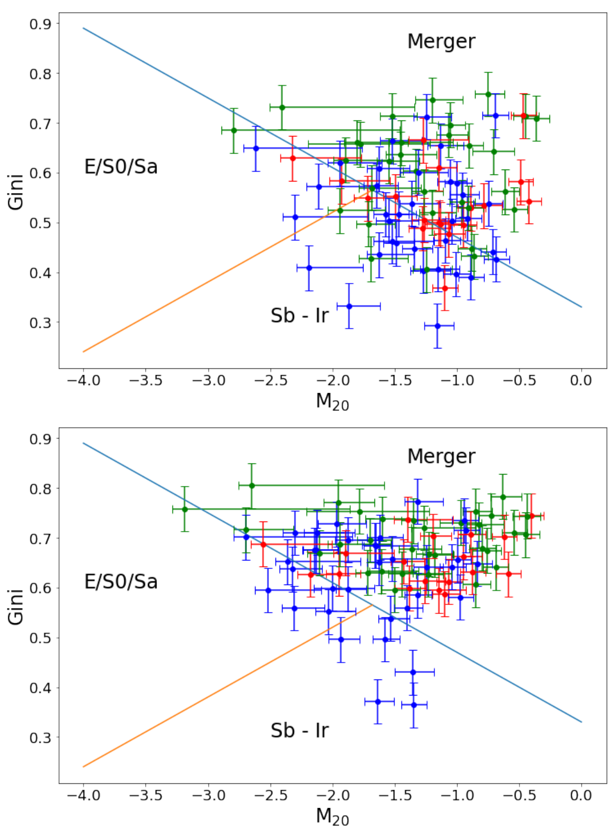

Figure 15: B-band plot (top) and I-band plot (bottom) of the sample, sorted by physical separation between the nuclei. Over 20 kpc is colored blue, 5-20 kpc is colored red, and 0-5 kpc is colored green.

We see from these plots that widely separated components are more likely to be classified as non-mergers. This is likely because these components have not yet interacted. As they get closer to their neighboring component(s), their morphologies will become tidally distorted, and they will likely move towards the merger region.

4.7 $\mathbf{I_{res}/I_{host}}$

Kim et al. (2013) determined a I_{res}/I_{host} fraction for each of the components, which quantifies how well the component fits a simple model such as a single nucleus. In particular, larger residuals yield larger I_{res}/I_{host} values. Figure 16 shows a plot of the components in Gini-M_{20} space, sorted by I_{res}/I_{host} fraction.

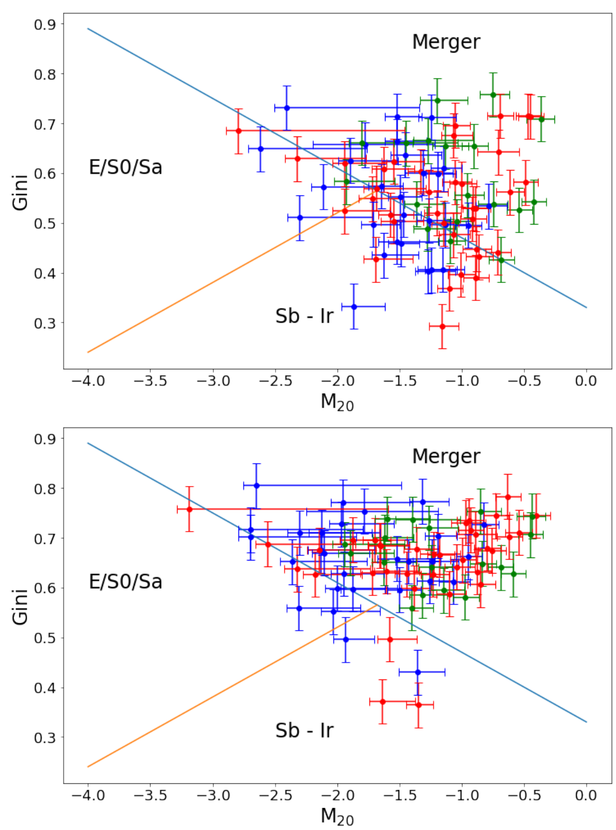

Figure 16: B-band plot (top) and I-band plot (bottom) of the sample, sorted by I_{res}/I_{host} fraction. 0-30% is colored blue, 30-45% is colored red, and over 45% is colored green.

We find that systems with low I_{res}/I_{host} tend to be more likely to be outliers, and there are very few outliers for components with high I_{res}/I_{host}. Based on this, we can conclude that a galaxy with an irregular morphology is more likely to be classified as a merger.

5 Conclusions

We plotted 56 galaxy merger systems in Gini-M_{20} space, and then expanded the sample to a total of 85 individual components of merger systems. We sorted these systems using a variety of different parameters and identified trends in the data. There are a few main takeaways from our analysis:

1. The I-band is a better metric for classifying LIRGs as mergers using Gini-M_{20} analysis.

2. Widely separated galaxies are easily classified as mergers when examining both components together, but examining widely separated components individually often leads to non-merger classifications.

3. Merging systems have more scatter in M_{20} as they evolve to later merger stages.

4. Components with morphologies that fit well to a simple model are more likely to be classified as non-mergers.

We found that the I-band images, in general, were more likely to be classified as mergers than their B-band counterparts. This is because we can see through more of the dust in LIRGs in the I-band images, which increases the brightness of the image and drives the Gini coefficient higher. At high redshift, we expect the surface brightness of the galaxies to decrease, as in the B-band images presented in Figure 11. This would drive the Gini coefficient downward and potentially shift the classification away from the merger region.

We found that widely separated galaxies were always classified as mergers when the components were analyzed together. This is because the wide separation causes a large portion of the emission to be located far from the center pixel, which drives the M_{20} value close to zero. We found that these galaxies were often classified as non-mergers when the components were analyzed individually. This is because many of these components have not yet interacted, and so the distortion features and increased star formation activity that are typical of mergers have not yet appeared. If we did not see these galaxies in close proximity to other galaxies, this analysis would be unable to determine that these components are part of a merger. Individual components would be even more difficult to identify as mergers at high redshift because of the low physical resolution.

We found that as merging systems evolve to later stages, there is more scatter in their M_{20} values. This is mostly because widely separated systems uniformly have M_{20} values close to zero, due to the distance from the bulk of the emission to the center of the system. This effect diminishes as the interaction evolves to later stages.

Finally, we found that galaxies with very regular morphologies, as in a model with a single nucleus, are more likely to be classified as non-mergers. This is because the bulk of the emission in these systems is concentrated in the center, whereas for irregularly shaped galaxies, the emission is often spread throughout the system.

6 Future Works

A future project would be to simulate the way these galaxies would appear at higher redshift, and to run the same analysis. This redshift technique was employed by Hibbard and Vacca (1997). If we can determine that this analysis holds at higher redshift, we would be able to use it to identify distant mergers and quantify how galaxy morphology changes as a function of cosmic time.

References

[1] Sanders, D. B. & Mirabel, I. F. 1996, ARAA, 34, 749. doi:10.1146/annurev.astro.34.1.749

[2] Murphy, E. J., Condon, J. J., Schinnerer, E., et al. 2011, ApJ, 737, 67. doi:10.1088/0004-637X/737/2/67

[3] Lotz, J. M., Davis, M., Faber, S. M., et al. 2008, ApJ, 672, 177. doi:10.1086/523659

[4] Petty, S. M., Armus, L., Charmandaris, V., et al. 2014, AJ, 148, 111. doi:10.1088/0004-6256/148/6/111

[5] Armus, L., Mazzarella, J. M., Evans, A. S., et al. 2009, PASP, 121, 559. doi:10.1086/600092

[6] Gini, C. 1912, Reprinted in Memorie di metodologica statistica (Ed. Pizetti E, Salvemini, T). Rome: Libreria Eredi Virgilio Veschi

[7] Lotz, J. M., Primack, J., & Madau, P. 2004, AJ, 128, 163. doi:10.1086/421849

[8] Sanders, D. B., Mazzarella, J. M., Kim, D.-C., et al. 2003, AJ, 126, 1607. doi:10.1086/376841

[9] Kim, D.-C., Evans, A. S., Vavilkin, T., et al. 2013, ApJ, 768, 102. doi:10.1088/0004-637X/768/2/102

[10] Haan, S., Surace, J. A., Armus, L., et al. 2011, AJ, 141, 100. doi:10.1088/0004-6256/141/3/100

[11] Larson, K. L., Sanders, D. B., Barnes, J. E., et al. 2016, ApJ, 825, 128. doi:10.3847/0004-637X/825/2/128

[12] Livermore, R. C., Jones, T. A., Richard, J., et al. 2015, MNRAS, 450, 1812. doi:10.1093/mnras/stv686

[13] Hibbard, J. E. & Vacca, W. D. 1997, AJ, 114, 1741. doi:10.1086/118603